CRYSTAL GROWTH & DESIGN

Article

pubs.acs.org/crystal

# Effect of Otoconial Proteins Fetuin A, Osteopontin, and Otoconin 90 on the Nucleation and Growth of Calcite

Mina Hong,[†,‡,§] K. Trent Moreland,[∥] Jiajun Chen,[§] Henry H. Teng,[‡] Ruediger Thalmann,*[,∥] and James J. De Yoreo*[,†]

[†]Physical Sciences Division, Pacific Northwest National Laboratory, Richland, Washington 99352, United States

[‡]Department of Chemistry, The George Washington University, Washington, D.C. 20052, United States

[§]The Molecular Foundry, Lawrence Berkeley National Laboratory, Berkeley, California 94720, United States

[∥]Department of Otolaryngology-Head and Neck Surgery, Washington University in St. Louis, St. Louis, Missouri 63110, United States

*S* *Supporting Information*

**ABSTRACT:** We investigated the roles of three proteins associated with the formation of otoconia including fetuin A, osteopontin (OPN), and otoconin 90 (OC90). In situ atomic force microscopy (AFM) studies of the effects of these proteins on the growth of atomic steps on calcite surfaces were performed to obtain insight into their effects on the growth kinetics. We also used scanning electron microscopy to examine the effects of these proteins on crystal morphology. All three proteins were found to be potent inhibitors of calcite growth, although fetuin A promoted growth at concentrations below about 40 nM and only became an inhibitor at higher concentrations. We then used in situ optical microscopy to observe calcite nucleation on films of these proteins adsorbed onto mica surfaces. By measuring the calcite nucleation rate as a function of supersaturation, the value of the interfacial energy that controls the free energy barrier to heterogeneous nucleation was determined for each protein. OPN and OC90 films led to significantly reduced interfacial energies as compared to the value for homogeneous calcite nucleation in bulk solution. The value for fetuin A was equal to that for bulk solution within experimental error. Zeta potential measurements showed all of the proteins possessed negative surface charge and varied in magnitude according to sequence fetuin A > OC90 > OPN. In addition, the interfacial energies exhibited an inverse scaling with the zeta potential. In analogy to previous measurements on polysaccharide films, this scaling indicates the differences between the proteins arise from the effect of protein surface charge on the solution−substrate interfacial energy.

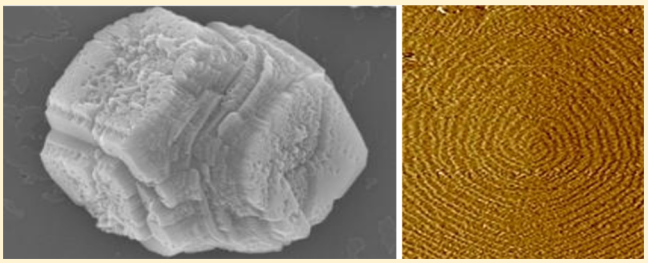

## INTRODUCTION

The process of biomineralization has been widely studied for many crystal systems. It is of great importance in both production of hard tissues and in mediating the interaction of biota with various terrestrial, aquatic, and marine environments. Moreover, biomineralization offers potential approaches to the formation of complex synthetic materials. Otoconia are small biominerals found in the saccule and utricle of the ear. As integral components of sense organs of linear acceleration and gravity, otoconia play an important role in maintaining spatial orientation and equilibrium.[1] Otoconia consist of an organic matrix, surrounded by a mineral shell composed of crystalline calcium carbonate.[2] The crystalline phase is one of three polymorphs: calcite (mammals and birds), aragonite (amphibians and fish), and vaterite (primitive jawfish).[3] It has been suggested by Pote and Ross that the selection of polymorphs is directed by specific major matrix proteins "unique to that polymorph",[4] though proof of that hypothesis is currently lacking. Otoconia in mammals are unique in that they are the only functional mammalian biomineral that consists of calcite instead of hydroxyapatite (calcium phosphate), which is the mineral phase of bone and teeth. In humans, calcitic otoconia are about 5−10 $\mu$m in length and exhibit triplanar (104) end facets. The otoconia are formed during embryogenesis with maturation occurring during a brief perinatal period after which they are believed to be static until demineralization begins with aging.[5] Decalcification occurs with increasing age and degrades the mineral resulting in loss of balance. Benign positional vertigo (BPV) often takes place as a result of displacement of otoconia into the semicircular canal due to head trauma or age-related otoconial fragmentation. In spite of the important role otoconia play in human balance and movement, little is known about their development, maintenance, and pathological processes at a molecular level.[6]

Previous studies suggest that the organic matrix of otoconia serves as a framework on which the calcite crystals deposit and

**Received:** July 3, 2014
**Revised:** October 22, 2014
**Published:** October 30, 2014

  

DOI: 10.1021/cg501001r
*Cryst. Growth Des.* 2015, 15, 129−136

grow.[7] In mammals and birds, the insoluble scaffold protein otolin-1 was identified to be the core protein of the matrix. Otolin-1, belonging to the C1q/TNF[8] and collagen superfamilies, is similar to the network forming type X collagen.[9] On the basis of the established role that collagens play in biomineralization and the recent demonstration that otolin-1 forms self-assembled networks in vitro,[7b] otolin-1 is expected to self-assemble in vivo into an extracellular scaffold structure essential for the directed nucleation and growth of the calcite crystal.[4,10] Otolin-1 appears to be recruited into the otoconial matrix by otoconin 90 (OC90),[11] which is the principal otoconial protein and accounts for more than 90% of the soluble phase.[12] OC90 is essential for the formation of this matrix and the deposition of otolin-1.[11] Otolin-1 has been reported to interact with OC90 when they are coexpressed.[10a] In the absence of OC90, the organic matrix was reported to be nearly absent, and the efficiency of crystal formation was reduced by 50%.[11a] In addition, OC90 was found to facilitate nucleation and control crystal size and morphology.[1,7b] In vitro coadministration of OC90 with otolin-1 to crystal growth solution produced synergistic effects on crystal morphology that resulted in calcite crystals resembling otoconia.[7b]

Many other proteins in the otoconia matrix have also been identified, including fetuin A, osteopontin (OPN), laminin alpha 3, Sparc-like protein 1, and myosin regulatory light polypeptide 9, all of which are calcium-binding proteins.[4,13] Fetuin A is abundant in serum[14] and was first identified in 1944 as a major protein component of bovine fetal serum.[15] It is a known inhibitor in the formation of calcium compounds, such as hydroxyapatite,[6] due to its strong Ca-binding property and accounts for about 50% of the capacity of serum to inhibit precipitation of Ca-salts, like calcium phosphate.[13] OPN also serves as an inhibitor of other Ca minerals including calcium oxalate,[16] calcite,[17] and hydroxyapatite.[18] Rounded and poorly formed facets of both the (010) and (101) faces of calcium oxalate and (104) faces of calcite indicate that OPN interacts with steps on the crystal faces.[16a,17] Phosphorylation of OPN was determined to be an important factor in the inhibitory effects.[16b,18] However, Zhao et al.[19] argued that OPN was not required for otoconia formation since no change of calcium concentration was observed in the ultrastructure in the absence of OPN.

We report results from atomic force microscopy (AFM), scanning electronic microscopy (SEM), optical microscopy, and electrophoretic light scattering (ELS) investigations into the role of three key otoconial proteins—fetuin A, OPN, and OC90—in the formation of calcite. In situ AFM studies of the effects of these proteins on the growth of atomic steps on calcite surfaces revealed interactions with the steps and the resulting control on growth kinetics and morphology. SEM images illustrated the relationship of changes in step kinetics to alterations in growth morphology. Optical microscopy enabled quantification of the kinetics of calcite nucleation on films of these proteins formed through deposition on mica surfaces. Interfacial energies controlling the thermodynamic barriers to nucleation were determined from measurements of calcite nucleation rate as a function of supersaturation. These interfacial energies were correlated with the charge density of the individual proteins as determined by zeta potential measurements obtained from ELS analysis.

## EXPERIMENTAL METHODOLOGY

**Protein Sources.** Commercial sources were used for fetuin A (Alpha 2 HS-Glycoprotein from American Research Product, Inc.) and OPN (Recombinant Mouse Osteopontin from R&D Systems, Inc.). The fetuin A was purified from human plasma, glycosylated and phosphorylated. The recombinant OPN was also phosphorylated, but details about the extent of phosphorylation were not available. Recombinant histidine tagged mouse OC90 protein was produced utilizing the Freestyle Max 293 expression system (Invitrogen) to transfect nonadherent human embryonic kidney (HEK293-F) cells with the expression plasmid pcDNA3.1-OC90-His per the manufacturer's directions. The transfected cells were incubated at 37 °C and 8% $CO_2$ for 7 days in Freestyle 293 Medium (Invitrogen). The medium containing the secreted protein was extracted from the cell culture, and the protein was purified chromatographically by affinity on an AKTA Purifier with a 1 mL HisTrap column (GE Healthcare). Total protein concentration was determined by the Bradford assay (BioRad). Purity and identity of the proteins were determined by Coomassie staining and Western blot using a 1:1000 dilution of polyclonal mouse anti-His C-terminal antibody (Abcam) following SDS-polyacrylamide gel electrophoresis on an AnyKD (BioRad) gel.

**Growth Experiments.** In situ measurements of the effects of all proteins on calcite monolayer step growth were carried out by AFM (Digital Instruments J scanner, Nanoscope IIIa and V controllers, Bruker Corporation, Billerica, MA). All measurements took place at 1 atm and room temperature (25 °C). Freshly cleaved calcite chips of optical-quality Iceland spar (Ward's Scientific, Chihuahua, Mexico) of approximately 2 mm × 2 mm × 1 mm in dimension were mounted in the fluid cell. Supersaturated calcite solutions were made by dissolving reagent sodium bicarbonate ($NaHCO_3$, Aldrich) and dehydrate calcium chloride ($CaCl_2$, Aldrich) into deionized water (18.2 mΩ). The supersaturation $\sigma$ was defined as

$$\sigma = \ln \Omega = \ln \frac{a_{Ca^{2+}} a_{CO_3^{2-}}}{K_{sp}}$$

and calculated by the commercial software PHREEQC to be 0.9 and 2.3.[20] pH was adjusted by adding HCl to the solutions to maintain it at ~7.44, which is close to the human physiological value. The ionic strength of all solutions was fixed at 0.2 M. Reactant solutions were continuously pumped through the fluid cell by a syringe pump at a flow rate of 60 mL/h, and all images were collected with silicon tips on silicon nitride cantilevers (AppNano Inc.). The crystal surfaces were allowed to grow for an hour before taking images to ensure quality and stability. Step velocities were calculated by measuring the change in apparent step orientations between continuous upward and downward AFM images collected in contact mode.[21] For each solution composition, the growth experiments were repeated at least three times, and step speed data were typically collected on two to three growth spirals in each experiment. The data points presented here represent an average of the measured values for each growth spiral. In addition, calcite crystals were grown by the carbonate diffusion method through the slow evaporation method of $NH_4HCO_3$ into a $CaCl_2$ solution as reported.[22] Briefly, they were grown on clean 12 mm glass coverslips, placed into wells of a cell culture dish containing 7.5 mM $CaCl_2$ solutions to which aliquots of the proteins had been added. The culture dish was covered with aluminum foil containing a few pinholes and placed into a sealed glass chamber containing $NH_4HCO_3$. Crystals were grown for 48 h and then examined with a JEOL JSM 6320F field emission scanning electron microscope at 5 kV after sputter coating with gold and palladium to increase the conductivity.

**Protein Adsorption.** 50 nM of each protein was dissolved in a 100 mM $CaCl_2$ solution. Freshly cleaved mica surfaces were incubated in solution for 8 h. After incubation, they were removed from solution, rinsed, and dried with compressed air. AFM tapping mode was used to examine the morphology of proteins adsorbed on the mica surfaces.

**Calcite Nucleation.** Nucleation of calcite on all three proteins films prepared as described above were investigated in situ using an inverted optical microscopy.[23] $CaCl_2$ and $NaHCO_3$ solutions at equal


DOI: 10.1021/cg501001r
Cryst. Growth Des. 2015, 15, 129−136

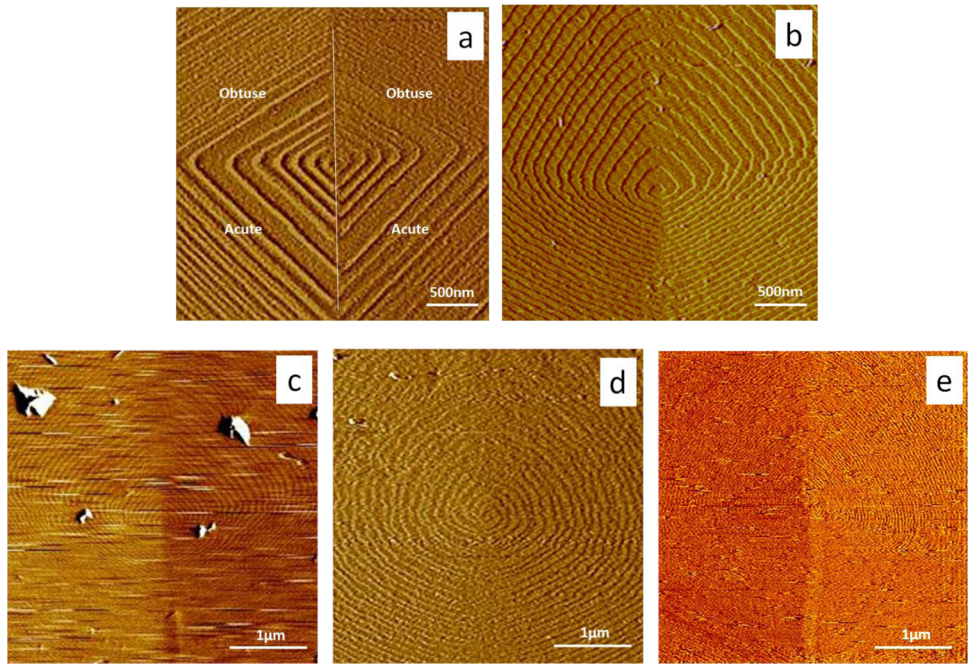


**Figure 1.** AFM images of calcite growth spirals in (a, b) protein-free solutions at $\sigma$ = 2.3 for (a) pH = 8.4 and (b) pH = 7.4; (c) 50 nM fetuin at pH = 7.4, (d) 80 nM OPN at pH = 7.4 and (e) 40 nM OC90 at pH = 7.4. All images were captured with obtuse steps up and acute sites at the bottom, as marked in (a). Panels (a) and (b) demonstrate the effect of pH on hillock morphology. Steps are partially covered or pinned by fetuin A, OPN, or OC90 in panels (c–e) respectively and the step velocity drops to about 50% of the original value. Image sizes are (a) and (b) 3 × 3 $\mu$m; (c) to (e) 4 × 4 $\mu$m. (Note that the differences in step spacing seen in (c–e) reflect the differences in step speed obtained with each protein.)

concentrations from 20 mM to 45 mM were mixed and pumped through the reaction cell at a flow rate of 120 mL/h. The location of nucleation events was recorded as the number density of nuclei vs time. This was repeated at multiple supersaturations ranging from 4.42 to 6.15.

**Protein Zeta Potential Measurement.** 50 nM of each protein was dissolved in a 1 mM $CaCl_2$ solution at pH 6.8. Zeta potential measurements of each protein were done by sz-100 nanoparticle analyzer (Horiba, Japan) at 1 atm and room temperature (25 °C).

## RESULTS

**Calcite Growth.** Growth hillocks on calcite (104) faces exhibit two crystallographically distinct types of steps, commonly referred to as "obtuse" and "acute". The difference in the kinetics of growth for the two types of steps is evident from the difference in the interstep spacing, which is a direct measure of the relative step speeds.[21a] Previous work at approximately pH 8.4[21a,24] showed that calcite growth hillocks consisted of straight steps with sharp corners, as seen in Figure 1a. The results presented here (Figure 1a,b) demonstrate that both types of steps become rounded when pH is decreased from 8.4 to 7.4, independent of the addition of proteins. Figure 1c–e showed the addition of protein at sufficiently high concentration can lead to further rounding, step pinning, or obscuring of the steps, presumably due to coverage of the surface by a protein film.

From sequences of images like those in Figure 1, we measured the dependence of step speed on protein concentration over the range required to see significant inhibition for all of the proteins (Figure 2). At the lowest protein concentrations used here, steps could be easily resolved and their speeds measured. As the protein concentration increased and steps became difficult to resolve (Figure 1c–e), step speeds could no longer be measured.

Decreases in the step speed were seen for both step-types as OC90 and OPN concentrations were increased. At an OC90 concentration of only 40 nM, step speeds dropped to <50% of the values in protein-free solution (Figure 2c), showing that OC90 is a potent inhibitor of calcite growth. The slightly stronger inhibition of the acute step over that of the obtuse steps is consistent with the change in crystal morphology seen in SEM images of crystals grown in the presence of the protein (Figure 3a,b) and is also consistent with the results of Lu et al.[1] and Moreland et al.[7b]

OPN had less impact on step speeds (Figure 2b) and crystal morphology (Figure 3c,d) than OC90 but still acted as an inhibitor of growth. OPN in concentrations from 1.59 to 3.82 $\mu$M caused a marked modification of crystal shape with increasing concentration (Figure 3c,d). Modification became evident at 1.59 $\mu$M with the (104) face becoming rounded and exhibiting a narrow ring-like band along the *c* axis (Figure 3c). These modifications significantly increased at 3.82 $\mu$M with strong rounding of the (104) faces becoming apparent.

In contrast to OC90 and OPN, fetuin A exhibited either enhancement or inhibition depending on protein concentration and solution supersaturation. At sufficiently high supersaturations (2.3) and low fetuin A concentration (<40 nM), an obvious increase in step speed was observed, while the protein exerted an inhibitory effect at concentrations greater than 40 nM (Figure 2a). As the protein concentration was further increased, fetuin A became an increasingly potent inhibitor. As shown in Figure 3d,e, the modification of crystal shape seen with increasing fetuin A concentration was similar to that observed with the other two proteins. At a concentration of 1.02 $\mu$M, a series of rounded macrosteps (Figure 3e) were observed on one side of the crystal while at concentrations of 2.04 $\mu$M (Figure 3f), significant rounding of acute steps and a broad ring-like band comprised of the (hk0) faces (i.e., parallel


DOI: 10.1021/cg501001r
*Cryst. Growth Des.* 2015, 15, 129–136

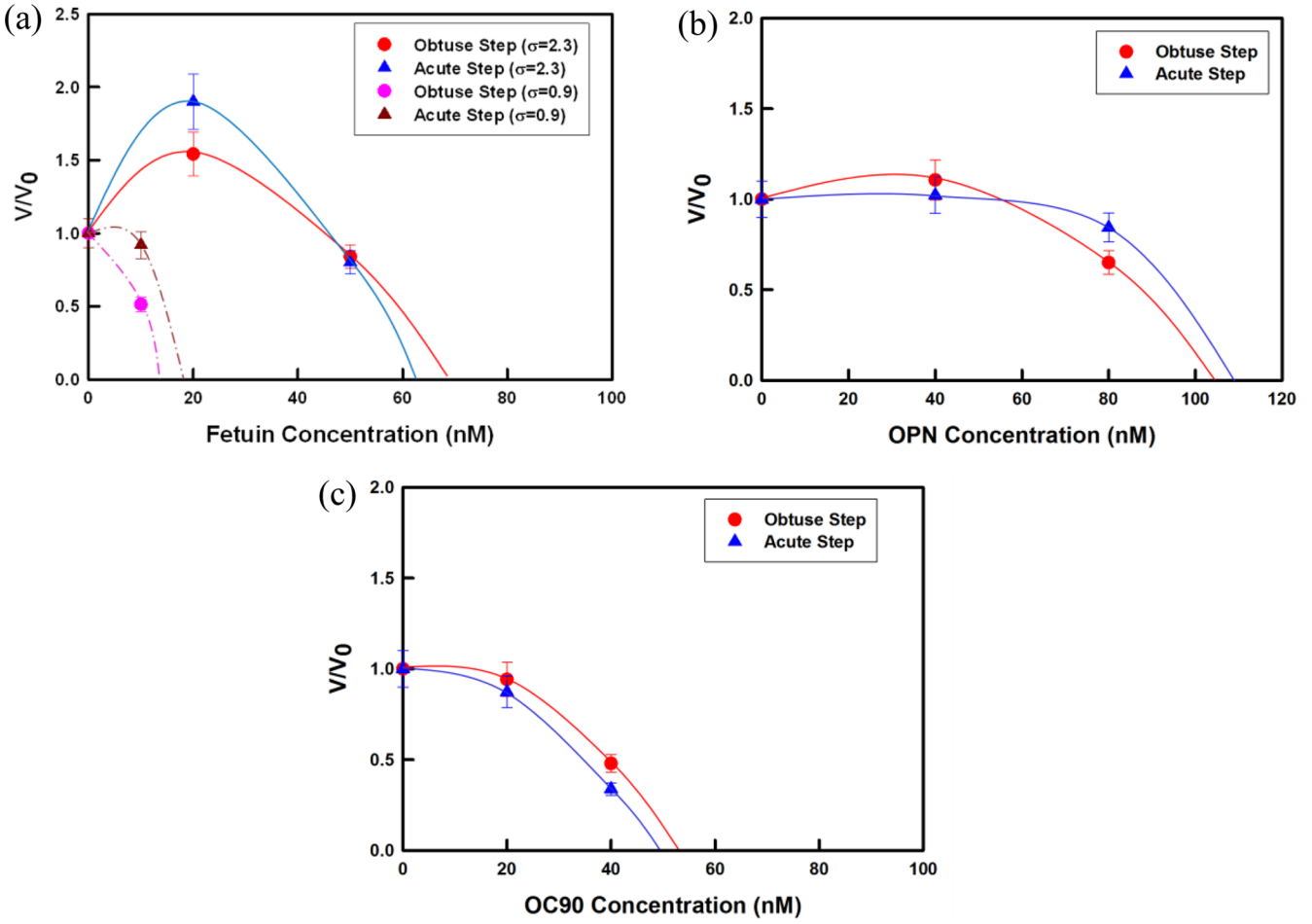


**Figure 2.** AFM measurements of step propagation rate vs concentration along both obtuse and acute directions for solutions containing (a) fetuin, (b) OPN, and (c) OC90. Normalized step speeds are given to emphasize the relative enhancement and/or inhibition and minimize the effects of inherent run-to-run variations in the step speed values. Lines are guides to the eye. Solid lines: $\sigma$ = 0.9; dashed lines in (a): $\sigma$ = 2.3. Error bars represent 10% of the measured value and are based upon error analyses in our previous investigations.[26a,34]

to the *c*-axis) were obtained, though the effects on morphology were less pronounced than with either OPN or OC90.

**Protein Adsorption.** Figure 4 shows the morphology of adsorbed fetuin, OPN, and OC90 on mica. After the same incubation time in the same electrolyte solution, all three formed isolated irregular islands on the mica surface. In addition, comparison with bare mica (Figure S1, Supporting Information) indicates that the surface was covered with protein, though the exact thickness is unknown. This is consistent with our expectation that these are soluble proteins and are not likely to form cross-linked filaments or three-dimensional networks as we observed previously for the otoconial protein otolin-1.[7b]

**Nucleation.** Using an in situ optical assay described previously,[23a,25] we measured the rate of calcite nucleation on adsorbed films of all of the proteins over a range of supersaturations. Figure 5a shows a typical dependence of nucleation rate $J_0$ on time $t$ for a given $\sigma$ (see also Figures S2 and S3, Supporting Information). Taking the linear portion of the curve as the quasi-steady state nucleation rate, we derived the dependence of $J_0$ on supersaturation. The results are plotted in Figure 5b as $\ln(J_0)$ vs the inverse supersaturation squared. In all cases, the rate increases with increasing $\sigma$ and exhibits a roughly linear dependence of $\ln(J_0)$ on $1/\sigma^2$.

**Zeta Potential Measurement.** We found that all three proteins had negative values of surface charge, which in the order of maximum to minimum were (absolute charge value): fetuin A (−30.1 ± 1.8 mV) > OC90 (−17.1 ± 2.1 mV) > OPN (−0.53 ± 0.23 mV).

## DISCUSSION

**Mechanisms of Growth Modification.** The propagation of steps on single crystal surfaces of calcite and other biomineral phases and the impact of peptides and proteins on that process have been explored in great detail over the past 15 years.[26] The salient point of those studies with respect to the current work is that soluble peptides and proteins often produce differential inhibition of calcite steps due to step-specific binding affinity that results in shape modification similar to that seen in Figure 3. The acute steps are often more susceptible to inhibition and induce an elongation of the crystals along the crystallographic (001) direction with a rounding of the (*hk*0) faces. In the case of aspartic acid-rich peptides from abalone nacre protein, Fu et al. related the effect on the morphology of the calcite atomic steps to the overall changes in crystal morphology.[26e,27] Given the fact that fetuin A, OPN, and OC90 have strong affinity to calcium, the results presented here indicate that each protein adsorbs to calcite steps and blocks calcium or carbonate ions from attaching to


DOI: 10.1021/cg501001r
*Cryst. Growth Des.* 2015, 15, 129−136

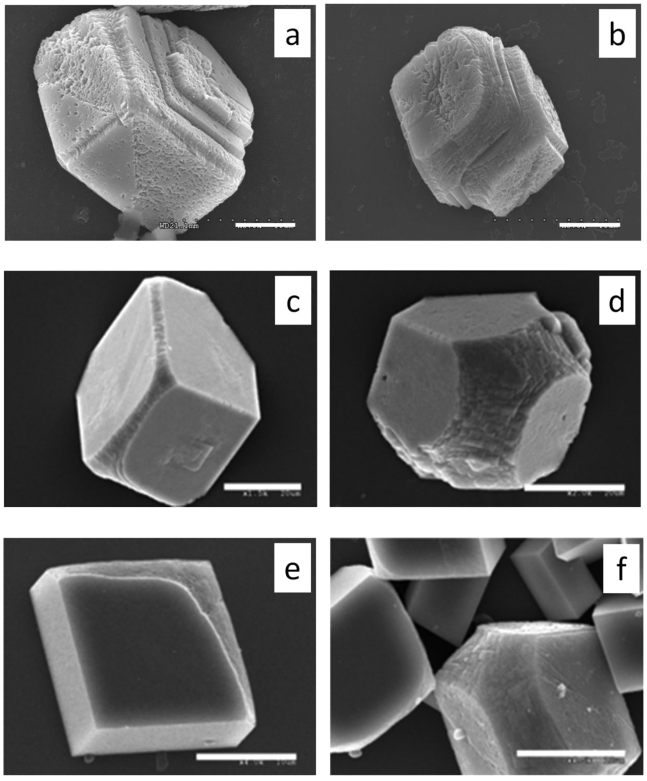


**Figure 3.** SEM images of calcite crystals modified by different proteins. (a) 0.5 $\mu$M OC90; (b) 1 $\mu$M OC90; (c) 1.59 $\mu$M recombinant mouse OPN; (d) 3.82 $\mu$M recombinant mouse OPN; (e) 1.02 $\mu$M human fetuin A; (f) 2.04 $\mu$M human fetuin A. Scale bar: a–c 20 $\mu$m; d–f 10 $\mu$m.

the kink sites.[26h,28] Step speed is thereby reduced at low protein concentrations, as seen in Figure 2. The morphologies seen in Figure 3 are indicative of rounding of the acute steps, which is usually associated with preferential binding to those steps. Though preferential inhibition is not discernible in the speeds of the steps at the much lower concentrations where the data must be collected, the preferential rounding is apparent in the hillock morphologies of Figure 1. Observation of overall inhibition and step rounding provides a rationale for the evolution in crystal shape and may provide insights to the source of the characteristic shape of otoconia.

The growth-enhancing regime observed with fetuin A (Figure 2a) has been reported in a number of protein–mineral systems[26f,g,29] and was explained as a catalytic process in which the activation barrier for solute addition to the crystal is reduced in the presence of the proteins at low concentration.[26f] In the growth-inhibiting regime, the critical concentration of fetuin A required to fully stop step propagation increases with solution supersaturation. This is due to the inverse relationship between calcite critical length and supersaturation, so less protein is needed to pin the edges and stop the steps at low supersaturation.[26g,28]

**Analysis of Nucleation Rates.** Classical nucleation theory (CNT) quantifies the steady state rate of nucleation $J_0(\mathrm{m}^{-2}\ \mathrm{s}^{-1})$ through[30]

$$J_0 = A\ \exp\left(-\frac{\Delta G^*}{k_B T}\right) \tag{1}$$

where $A$ is a kinetic prefactor, $k_B$ is Boltzmann constant, and $T$ is temperature. $\Delta G^*$ is the free energy barrier to the formation of a critical size nucleus given by

$$\Delta G^* = \frac{F\omega^2\alpha^3}{\sigma^2 k_B^2 T^2} \tag{2}$$

Here $F$ is the shape-dependent factor for crystal nuclei, $\omega$ is the molecular volume of the crystal, which equals $6.13 \times 10^{-29}$ m$^3$ per molecule for calcite,[31] and $\alpha$ is the net interfacial energy. Combining eqs 1 and 2 gives

$$\ln(J_0) = \ln(A) - B\left(\frac{1}{\sigma^2}\right) \tag{3}$$

in which the slope, $B$, is given by

$$B = \frac{F\omega^2\alpha^3}{k_B^3 T^3} \tag{4}$$

Thus, for any value of $\sigma$, $\Delta G^*$ can be obtained directly from $B$ through

$$\Delta G^* = \frac{B k_B T}{\sigma^2} \tag{5}$$

The shape factor $F$ depends on the orientation of the nucleus. However, it does not change significantly from one to another.[23a] For all protein films, we observed calcite nucleation with random orientations.

Using a shape factor of 17, which is the average for calcite rhombs nucleating on the (012) and (104) faces, we estimate from the slopes in Figure 5b that the values of $\alpha$ range from a low of 77 ± 0.5 mJ/m$^2$ for OPN to a high of 117 ± 1.4 mJ/m$^2$ for fetuin A, with the OC90 film falling at an intermediate values of 96 ± 1.1 mJ/m$^2$ (Table 1). The values for

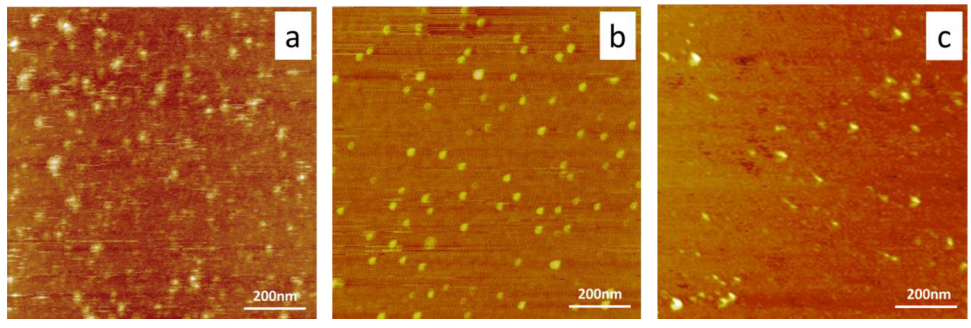


**Figure 4.** Ex situ AFM height images (1.0 × 1.0 $\mu$m) following absorption of (a) 50 nM fetuin A (b) 50 nM OPN, and (c) 50 nM OC90 on freshly cleaved mica. Image sizes are (a) to (c) 1 × 1 $\mu$m.



DOI: 10.1021/cg501001r
*Cryst. Growth Des.* 2015, 15, 129–136

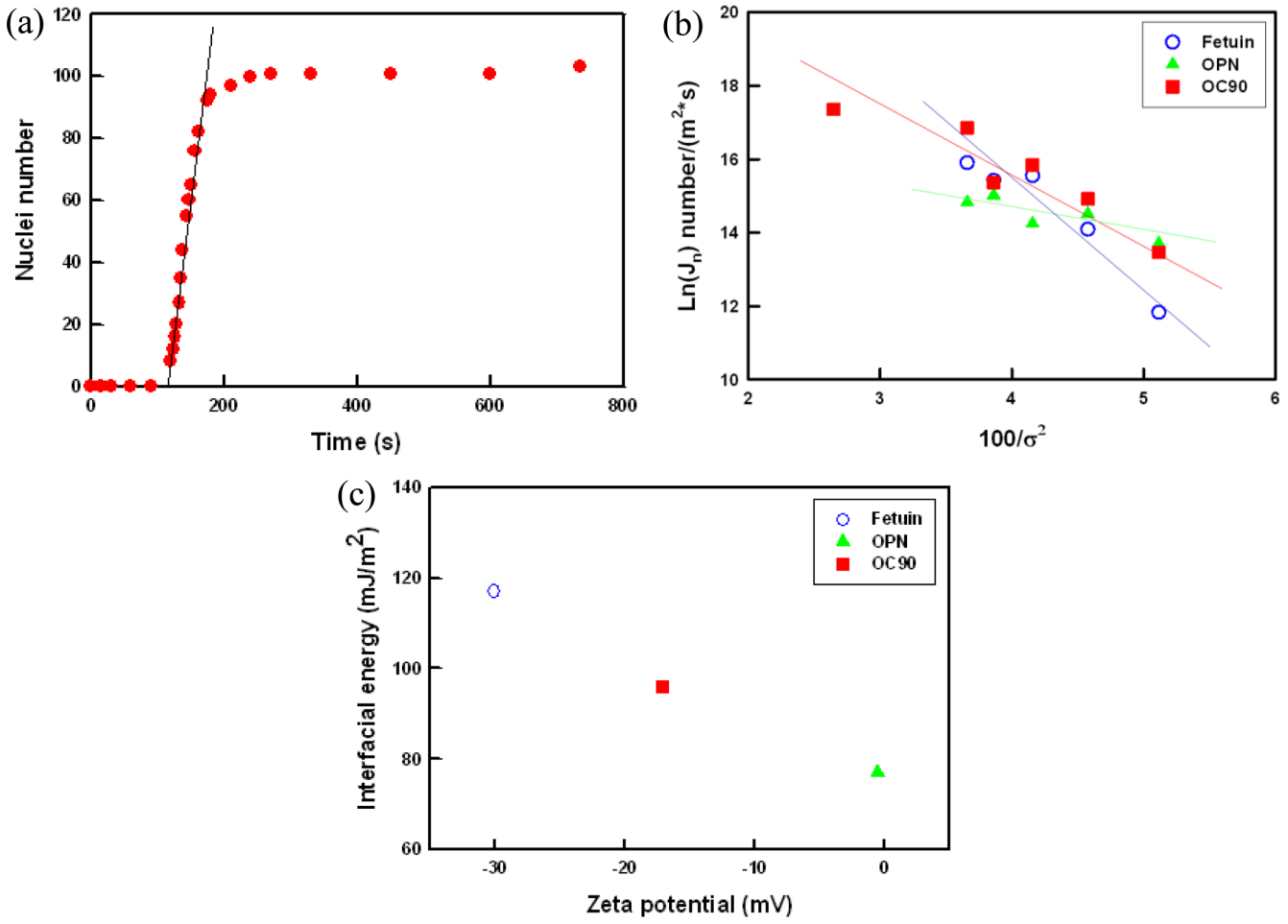


**Figure 5.** Dependence of nucleation rate on time and supersaturation. (a) An example of number of calcite nuclei vs time on a film of OC90 at $\sigma$ = 4.90. The slope of the linear portion of the curve for each supersaturation corresponds to the steady-state nucleation rate, $J_0$. (b) Natural logarithm of the steady-state nucleation rate vs the inverse of the supersaturation squared exhibiting the linear relationship predicted by eq 3 for all substrates. The slope of the line $B$ is proportional to the substrate-specific free energy barrier. (c) The zeta potential exhibiting an inverse linear relationship between protein surface charge density and interfacial energy.

**Table 1. Slopes B and Interfacial Free Energies $\alpha$ on the Different Protein Substrates**[a]

| substrate | $B$ | $\alpha$ (mJ/m$^2$) |
|---|---|---|
| none (homogeneous) | | 109 |
| fetuin | −1456 | 117 ± 1.4 |
| OPN | −411 | 77 ± 0.5 |
| OC90 | −819 | 96 ± 1.1 |

[a]Calculations of $\alpha$ are based on the assumption of rhombohedral shaped nuclei. All the properties are protein dependent.

heterogeneous nucleation on OPN and OC90 are substantially less than that for homogeneous nucleation in the bulk solution where $\alpha$ = 109 mJ/m$^2$.[23a,32] This reduction arises from the interaction between the nucleating crystal and the substrate as well as the interaction between the solution and substrate.[25,33] For heterogeneous nucleation, the net interfacial energy is determined by three independent interfacial energies for the crystal−liquid ($\alpha_{CL}$), substrate−crystal ($\alpha_{SC}$), and liquid−substrate ($\alpha_{LS}$) interfaces. These are related by the expression:

$$\alpha = \alpha_{CL} + h(\alpha_{SC} - \alpha_{LS}) \quad (6)$$

where $h$ is a constant that depends on nucleus shape (e.g., $h$ = 0.525 for a calcite rhomb nucleating on the (012) face[23a] and 0.276 for the (104) face). $\alpha_{CL}$ can be treated as constant in our cases so the differences in interfacial energy are controlled by the relative values of $\alpha_{SC}$ and $\alpha_{LS}$.

The value of $\alpha_{SC}$ is determined by the strength of crystal binding to the substrate,[33] while $\alpha_{LS}$ is largely controlled by surface charge density, surface hydrophilicity, or hydrophobicity.[25] From eq 6 we infer that $(\alpha_{SC} - \alpha_{LS})_{fetuin} > (\alpha_{SC} - \alpha_{LS})_{OC90} > (\alpha_{SC} - \alpha_{LS})_{OPN}$. In the case of polysaccharides reported by Giuffre et al.,[25] higher negative charge density resulted in lower $\alpha_{LS}$ and thus larger $\alpha$ and higher $\alpha$ nucleation barrier. In contrast, in the case of organothiol self-assembled monolayers. Hamm et al.[33] found that larger values of the binding energy between the substrate and the crystal resulted in lower values of $\alpha_{SC}$ and thus smaller $\alpha$. The zeta potential measurements indicate that the proteins exhibit a similar control to that seen for the polysaccharides. As Figure 5c shows, the zeta potential exhibits an inverse linear relationship between the surface charge density and the interfacial energy, with the large negative zeta potential of fetuin A leading to the lowest value of $\alpha$ and the small zeta potential of OPN giving the largest value of $\alpha$. (It is worth noting that analysis of net charge at pH 7.44 based on sequence alone gives a relative ranking that is exactly reversed from that determined by zeta potential, showing that structural factors impact the relative number of


DOI: 10.1021/cg501001r
Cryst. Growth Des. 2015, 15, 129−136

charged residues exposed at the surfaces of the proteins and highlighting the utility of the zeta potential data.)

The magnitude of the changes in the free energy barrier is even more significant than the changes in $\alpha$, because the barrier contains $\alpha^3$ (eq 1). Moreover, because the barrier enters into the rate $J_0$ as the argument of an exponential, the increase in nucleation rates due the observed differences in $\alpha$ can be dramatic. For example, at a supersaturation equal to 5.37, taking all other terms in eqs 1 and 2 to be equal, a drop in $\alpha$ from 109 to 77 mJ/m$^2$ would result in an increase in nucleation rates by a factor of $3.75 \times 10^{11}$, showing that OPN and OC90 may serve as potent promoters of nucleation.

## CONCLUSIONS

The results reported here demonstrate that fetuin A, OPN, and OC90 are inhibitors of calcite growth through step pinning, presumably due to their high calcium binding affinity. The dependence of nucleation rate on supersaturation shows that the interfacial free energy of calcite on fetuin A (117 mJ/m$^2$) is similar to that for calcite in bulk solution, while OPN and OC90 reduce it to 72.46 and 91.21 mJ/m$^2$, respectively. Zeta potential measurements reveal that fetuin A carries more negative charge than OC90 and OPN. Given the previously demonstrated relationship between the surface charge density and solution−substrate interfacial energy, these results indicate that the variation in interfacial energy observed here is due to the differences in protein surface charge density, which impacts the affinity of the substrates for the aqueous solution (i.e., the hydrophilicity). The consequence is that while fetuin A presents a higher free energy barrier to nucleation than the bulk solution, OPN and OC90 present much lower free energy barriers.

## ASSOCIATED CONTENT

### Supporting Information

Figure S1: AFM image of bare mica surface. Figure S2: Time sequence of optical images showing dependence of nucleation density on time for OPN. Figure S3: Plot showing number density of nuclei vs. time for fetuin. This material is available free of charge via the Internet at http://pubs.acs.org.

## AUTHOR INFORMATION

### Corresponding Authors

*(J.J.D.) E-mail: james.deyoreo@pnnl.gov.
*(R.T.) E-mail: thalmannr@ent.wustl.edu.

### Notes

The authors declare no competing financial interest.

## ACKNOWLEDGMENTS

This work was supported by NIH/NIDCD grant number RO1 DC011614. The funders had no role in study design, data collection and analysis, decision to publish, or preparation of the manuscript. This research was performed at Pacific Northwest National Laboratory, which is operated by Battelle for the U.S. Department of energy under Contract DE-AC05-76RL01830, at the Molecular Foundry, Lawrence Berkeley National Laboratory, which is supported by the Office of Basic Energy Sciences, Scientific User Facilities Division, and at the Washington University in St. Louis, Department of Otolaryngology. The authors would like to acknowledge Washington University in St. Louis, Department of Otolaryngology's Electron Microscopy Core.

## REFERENCES

(1) Lu, W. F.; Zhou, D.; Freeman, J. J.; Thalmann, I.; Ornitz, D. M.; Thalmann, R. In vitro effects of recombinant otoconin 90 upon calcite crystal growth. Significance of tertiary structure. *Hearing Res.* **2010**, *268* (1−2), 172−183.

(2) Lins, U.; Farina, M.; Kurc, M.; Riordan, G.; Thalmann, R.; Thalmann, I.; Kachar, B. The otoconia of the guinea pig utricle: Internal structure, surface exposure, and interactions with the filament matrix. *J. Struct. Biol.* **2000**, *131* (1), 67−78.

(3) Ross, M. D.; Pote, K. G. Some properties of otoconia. *Philos. Trans. R. Soc. London, B* **1984**, *304* (1121), 445−452.

(4) Pote, K. G.; Ross, M. D. Each otoconia polymorph has a protein unique to that polymorph. *Comp. Biochem. Physiol., Part B: Biochem. Mol. Biol.* **1991**, *98* (2−3), 287−295.

(5) (a) Ross, M. D.; Peacor, D.; Johnsson, L. G.; Allard, L. F. Observations on normal and degenerating human otoconia. *Ann. Otol. Rhinol. Laryngol.* **1976**, *85* (3), 310−326. (b) Lim, D. J. Otocnia health and disease - A review. *Ann. Otol. Rhinol. Laryngol.* **1984**, *93* (4), 17−24. (c) Anniko, M.; Ylikoski, J.; Wroblewski, R. Microprobe analysis of human otoconia. *Acta Oto-Laryngol.* **1984**, *97* (3−4), 283−289.

(6) Schinke, T.; Amendt, C.; Trindl, A.; Poschke, O.; MullerEsterl, W.; JahnenDechent, W. The serum protein alpha(2)-HS glycoprotein/fetuin inhibits apatite formation in vitro and in mineralizing calvaria cells - A possible role in mineralization and calcium homeostasis. *J. Biol. Chem.* **1996**, *271* (34), 20789−20796.

(7) (a) Xu, Y. F.; Zhang, H.; Yang, H.; Zhao, X.; Lovas, S.; Lundberg, Y. W. Expression, Functional, and Structural Analysis of Proteins Critical for Otoconia Development. *Dev. Dyn.* **2010**, *239* (10), 2659−2673. (b) Moreland, K. T.; Hong, M. N.; Lu, W. F.; Rowley, C. W.; Ornitz, D. M.; De Yoreo, J. J.; Thalmann, R. In Vitro Calcite Crystal Morphology Is Modulated by Otoconial Proteins Otolin-1 and Otoconin-90. *PLoS One* **2014**, *9* (4), 8.

(8) Deans, M. R.; Peterson, J. M.; Wong, G. W. Mammalian Otolin: A Multimeric Glycoprotein Specific to the Inner Ear that Interacts with Otoconial Matrix Protein Otoconin-90 and Cerebellin-1. *PLoS One* **2010**, *5* (9), 15.

(9) Yang, H.; Zhao, X.; Xu, Y. F.; Wang, L. L.; He, Q. Y.; Lundberg, Y. W. Matrix Recruitment and Calcium Sequestration for Spatial Specific Otoconia Development. *PLoS One* **2011**, *6* (5), 12.

(10) (a) Deans, M. R.; Peterson, J. M.; Wong, G. W. Mammalian Otolin: A Multimeric Glycoprotein Specific to the Inner Ear that Interacts with Otoconial Matrix Protein Otoconin-90 and Cerebellin-1. *PLoS One* **2010**, *5* (9), 10.1371/journal.pone.0012765. (b) Ornitz, D. M.; Bohne, B. A.; Thalmann, I.; Harding, G. W.; Thalmann, R. Otoconial agenesis in tilted mutant mice. *Hearing Res.* **1998**, *122* (1−2), 60−70.

(11) (a) Zhao, X.; Yang, H.; Yamoah, E. N.; Lundberg, Y. W. Gene targeting reveals the role of Oc90 as the essential organizer of the otoconial organic matrix. *Dev. Biol.* **2007**, *304* (2), 508−524. (b) Murayama, E.; Herbomel, P.; Kawakami, A.; Takeda, H.; Nagasawa, H. Otolith matrix proteins OMP-1 and Otolin-1 are necessary for normal otolith growth and their correct anchoring onto the sensory maculae. *Mech. Dev.* **2005**, *122* (6), 791−803.

(12) (a) Verpy, E.; Leibovici, M.; Petit, C. Characterization of otoconin-95, the major protein of murine otoconia, provides insights into the formation of these inner ear biominerals. *Proc. Natl. Acad. Sci. U.S.A.* **1999**, *96* (2), 529−534. (b) Wang, Y. X.; Kowalski, P. E.; Thalmann, I.; Ornitz, D. M.; Mager, D. L.; Thalmann, R. Otoconin-90, the mammalian otoconial matrix protein, contains two domains of homology to secretory phospholipase A(2). *Proc. Natl. Acad. Sci. U.S.A.* **1998**, *95* (26), 15345−15350.

(13) Thalmann, I.; Hughes, I.; Tong, B. D.; Ornitz, D. M.; Thalmann, R. Microscale analysis of proteins in inner ear tissues and fluids with emphasis on endolymphatic sac, otoconia, and organ of Corti. *Electrophoresis* **2006**, *27* (8), 1598−1608.

(14) Jahnen-Dechent, W.; Schafer, C.; Ketteler, M.; McKee, M. D. Mineral chaperones: a role for fetuin-A and osteopontin in the inhibition and regression of pathologic calcification. *J. Mol. Med.* **2008**, *86* (4), 379−389.



DOI: 10.1021/cg501001r
*Cryst. Growth Des.* 2015, 15, 129−136

(15) Pedersen, K. O. Fetuin, a new globulin isolated from serum. *Nature* **1944**, *154*, 575−575.
(16) (a) Wang, L. J.; Zhang, W.; Qiu, S. R.; Zachowicz, W. J.; Guan, X. Y.; Tang, R. K.; Hoyer, J. R.; De Yoreo, J. J.; Nancollas, G. H. Inhibition of calcium oxalate monohydrate crystallization by the combination of citrate and osteopontin. *J. Cryst. Growth* **2006**, *291* (1), 160−165. (b) Hoyer, J. R.; Asplin, J. R.; Otvos, L. Phosphorylated osteopontin peptides suppress crystallization by inhibiting the growth of calcium oxalate crystals. *Kidney Int.* **2001**, *60* (1), 77−82.
(17) Chien, Y. C.; Hincke, M. T.; Vali, H.; McKee, M. D. Ultrastructural matrix-mineral relationships in avian eggshell, and effects of osteopontin on calcite growth in vitro. *J. Struct. Biol.* **2008**, *163* (1), 84−99.
(18) Pampena, D. A.; Robertson, K. A.; Litvinova, O.; Lajoie, G.; Goldberg, H. A.; Hunter, G. K. Inhibition of hydroxyapatite formation by osteopontin phosphopeptides. *Biochem. J.* **2004**, *378*, 1083−1087.
(19) Zhao, X.; Jones, S. M.; Thoreson, W. B.; Lundberg, Y. W. Osteopontin is not critical for otoconia formation or balance function. *J. Assoc. Res. Otolaryngol.* **2008**, *9* (2), 191−201.
(20) Parkhurst, D. L.; Appelo, C. A. J. User's guide to PHREEQC (Version 2)--a computer program for speciation, batch-reaction, one-dimensional transport, and inverse geochemical calculations, U.S. Geological Survey Water, Resources Investigations Report, 1999; p 312.
(21) (a) Teng, H. H.; Dove, P. M.; Orme, C. A.; De Yoreo, J. J. Thermodynamics of calcite growth: Baseline for understanding biomineral formation. *Science* **1998**, *282* (5389), 724−727. (b) De Yoreo, J. J.; Land, T. A.; Rashkovich, L. N.; Onischenko, T. A.; Lee, J. D.; Monovskii, O. V.; Zaitseva, N. P. The effect of dislocation cores on growth hillock vicinality and normal growth rates of KDP {1 0 1} surfaces. *J. Cryst. Growth* **1997**, *182* (3−4), 442−460.
(22) Albeck, S.; Aizenberg, J.; Addadi, L.; Weiner, S. Iinteracions of various skeletal intracrystalline components with calcite crystals. *J. Am. Chem. Soc.* **1993**, *115* (25), 11691−11697.
(23) (a) Hu, Q.; Nielsen, M. H.; Freeman, C. L.; Hamm, L. M.; Tao, J.; Lee, J. R. I.; Han, T. Y. J.; Becker, U.; Harding, J. H.; Dove, P. M.; De Yoreo, J. J. The thermodynamics of calcite nucleation at organic interfaces: Classical vs. non-classical pathways. *Faraday Discuss.* **2012**, *159*, 509−523. (b) Habraken, W.; Tao, J. H.; Brylka, L. J.; Friedrich, H.; Bertinetti, L.; Schenk, A. S.; Verch, A.; Dmitrovic, V.; Bomans, P. H. H.; Frederik, P. M.; Laven, J.; van der Schoot, P.; Aichmayer, B.; de With, G.; De Yoreo, J. J.; Sommerdijk, N. Ion-association complexes unite classical and non-classical theories for the biomimetic nucleation of calcium phosphate. *Nat. Commun.* **2013**, *4*, 12.
(24) Hong, M.; Teng, H. H. Implications of solution chemistry dffects: Direction-specific restraints on the step kinetics of calcite growth. *Geochim. Cosmochim. Acta* **2014**, *141*, 228−239.
(25) Giuffre, A. J.; Hamm, L. M.; Han, N.; De Yoreo, J. J.; Dove, P. M. Polysaccharide chemistry regulates kinetics of calcite nucleation through competition of interfacial energies. *Proc. Natl. Acad. Sci. U.S.A.* **2013**, *110* (23), 9261−9266.
(26) (a) Teng, H. H.; Dove, P. M.; De Yoreo, J. J. Kinetics of calcite growth: Surface processes and relationships to macroscopic rate laws. *Geochim. Cosmochim. Acta* **2000**, *64* (13), 2255−2266. (b) Orme, C. A.; Noy, A.; Wierzbicki, A.; McBride, M. T.; Grantham, M.; Teng, H. H.; Dove, P. M.; De Yoreo, J. J. Formation of chiral morphologies through selective binding of amino acids to calcite surface steps. *Nature* **2001**, *411* (6839), 775−779. (c) Guo, S. W.; Ward, M. D.; Wesson, J. A. Direct visualization of calcium oxalate monohydrate crystallization and dissolution with atomic force microscopy and the role of polymeric additives. *Langmuir* **2002**, *18* (11), 4284−4291. (d) Qiu, S. R.; Wierzbicki, A.; Orme, C. A.; Cody, A. M.; Hoyer, J. R.; Nancollas, G. H.; Zepeda, S.; De Yoreo, J. J. Molecular modulation of calcium oxalate crystallization by osteopontin and citrate. *Proc. Natl. Acad. Sci. U.S.A.* **2004**, *101* (7), 1811−1815. (e) Fu, G.; Valiyaveettil, S.; Wopenka, B.; Morse, D. E. CaCO3 biomineralization: Acidic 8-kDa proteins isolated from aragonitic abalone shell nacre can specifically modify calcite crystal morphology. *Biomacromolecules* **2005**, *6* (3), 1289−1298. (f) Elhadj, S.; De Yoreo, J. J.; Hoyer, J. R.; Dove, P. M. Role of molecular charge and hydrophilicity in regulating the kinetics of crystal growth. *Proc. Natl. Acad. Sci. U.S.A.* **2006**, *103* (51), 19237−19242. (g) De Yoreo, J. J.; Wierzbicki, A.; Dove, P. M. New insights into mechanisms of biomolecular control on growth of inorganic crystals. *CrystEngComm* **2007**, *9* (12), 1144−1152. (h) Maruyama, M.; Tsukamoto, K.; Sazaki, G.; Nishimura, Y.; Vekilov, P. G. Chiral and Achiral Mechanisms of Regulation of Calcite Crystallization. *Cryst. Growth Des.* **2009**, *9* (1), 127−135. (i) Friddle, R. W.; Weaver, M. L.; Qiu, S. R.; Wierzbicki, A.; Casey, W. H.; De Yoreo, J. J. Subnanometer atomic force microscopy of peptide-mineral interactions links clustering and competition to acceleration and catastrophe. *Proc. Natl. Acad. Sci. U.S.A.* **2010**, *107* (1), 11−15.
(27) Fu, G.; Qiu, S. R.; Orme, C. A.; Morse, D. E.; De Yoreo, J. J. Acceleration of calcite kinetics by abalone nacre proteins. *Adv. Mater.* **2005**, *17* (22), 2678−2683.
(28) De Yoreo, J. J.; Zepeda-Ruiz, L. A.; Friddle, R. W.; Qiu, S. R.; Wasylenki, L. E.; Chernov, A. A.; Gilmer, G. H.; Dove, P. M. Rethinking Classical Crystal Growth Models through Molecular Scale Insights: Consequences of Kink-Limited Kinetics. *Cryst. Growth Des.* **2009**, *9* (12), 5135−5144.
(29) Weaver, M. L.; Qiu, S. R.; Hoyer, J. R.; Casey, W. H.; Nancollas, G. H.; De Yoreo, J. J. Surface Aggregation of Urinary Proteins and Aspartic Acid-Rich Peptides on the Faces of Calcium Oxalate Monohydrate Investigated by In Situ Force Microscopy. *Calcif. Tissue Int.* **2009**, *84* (6), 462−473.
(30) (a) Turnbull, D.; Fisher, J. C. Rater of nucleation in condensed systems. *J. Chem. Phys.* **1949**, *17* (1), 71−73. (b) Markove, I. V. *Crystal Growth for Beginners: Fundamentals of Nucleation, Crystal Growth and Epitaxy*; World Scientific: Singapore, 2003.
(31) Davis, K. J.; Dove, P. M.; De Yoreo, J. J. The role of $Mg^{2+}$ as an impurity in calcite growth. *Science* **2000**, *290* (5494), 1134−1137.
(32) Sohnel, O.; Mullin, J. W. Method for determination of precipitation induction periods. *J. Cryst. Growth* **1978**, *44* (4), 377−382.
(33) Hamm, L. M.; Giuffre, A. J.; Han, N.; Tao, J. H.; Wang, D. B.; De Yoreo, J. J.; Dove, P. M. Reconciling disparate views of template-directed nucleation through measurement of calcite nucleation kinetics and binding energies. *Proc. Natl. Acad. Sci. U.S.A.* **2014**, *111* (4), 1304−1309.
(34) Land, T. A.; DeYoreo, J. J.; Lee, J. D. An in-situ AFM investigation of canavalin crystallization kinetics. *Surf. Sci.* **1997**, *384* (1−3), 136−155.


DOI: 10.1021/cg501001r
*Cryst. Growth Des.* 2015, 15, 129−136